Flexible Ta_2O_5/WO_3-Based Memristor Synapse for Wearable and Neuromorphic Applications

Sailesh Rajasekaran, Firman Mangasa Simanjuntak, *Member, IEEE*, Sridhar Chandrasekaran, Debashis Panda, Aftab Saleem, and Tseung-Yuen Tseng, *Fellow, IEEE*

***Abstract*—In this letter, Ta_2O_5/WO_3 double-layer wearable memristor synapse has excellent recognition accuracy (97%) for just 12 epochs compared to the single-layer device (83%). The insertion of an ultra-thin WO_3 layer modulates the oxygen vacancy distribution in Ta_2O_5 and induces digital-to-analog switching behavior. Excellent AC endurance of ($>10^9$ cycles) under 2 mm extreme bending, a rapid speed (25 ns), reliable bending endurance for 10^4 cycles with 4 mm bending, stable retention ($>10^6$ s) up to 200°C, and water-resistant behavior are achieved. The potentiation, and depression having outstanding nonlinearity (0.64) is obtained. The Ta_2O_5/WO_3 design is a promising candidate for wearable neuromorphic applications due to its wearability, flexibility, lightweight, low cost and environmental friendly fabrication.**

***Index Terms*—Artificial neural networks, flexible electronics, resistive synapse, face recognition.**

I. INTRODUCTION

ARTIFICIAL neural networks (ANN) is developed to make machines capable of performing complex intelligent tasks such as cognitive learning and real-time decision making; memristor-based ANN promises a lower power consumption, faster, and denser neuromorphic hardware than the traditional von Neumann computing architecture [1]–[4]. The memristor mimics mammalian synaptic functionalities of the brain with significant architectonic advantages such as two-terminal simple fabrication, low heat dissipation, and fully adjustable non-volatility [5]–[7]. Artificial synapses made with analog memristor should be capable of performing good synaptic plasticity (gradual potentiation and depression with large conductance states) to ensure fast computation [8]–[11]. Artificial synaptic devices with less than 100 modulated conductance states may not be sufficient for efficient ANNs [12], [13]. Indeed, significant efforts to enhance the synaptic plasticity have been made in the last decade, such as by modulating the pulse scheme [13], [14], employing 2D materials [15], [15], embedding nanolayer [16] or nanoparticle [17], and adding a dopant [18] or barrier layer [19]. However, most of these techniques are fabricated on rigid substrates and not adoptable for wearable applications. The critical challenge in wearable electronics is that the devices should be able to endure extreme flexibility, high-temperature stability and suitable for outdoor environment (such as water resistant). Recent work on resistive memory suggested that a compact 2-dimensional layer was required to achieve water resistant capability [20]; nonetheless, the fabrication flow for this design is complex and time consuming, and moreover, it does not offer flexibility and synaptic capabilities as well as high density design.

In this work, we propose water resistant $TaN/Ta_2O_5/WO_3/Pt$ design for high performance flexible memristor synapse for wearable electronics employing the CMOS compatibility, good reliability, and suitability of the TaO_x materials for outdoor environments [21]. We also demonstrate that inserting a WO_3 layer can enhance the electrical performance and mechanical flexibility of the device. Our device can withstand extreme bending while maintaining long endurance, ns regime rapid switching, high temperature retention, multibit, and excellent synaptic performance for high speed neuromorphic computation application. The proposed design is found to be superior than other TaO_x-based memories [22]. Thus, the double layer device has the basic requirement for wearable neuromorphic hardware.

II. DEVICE FABRICATION

We fabricated $TaN/Ta_2O_5/WO_3/Pt$ (DL) (shown schematically in Fig. 1(a)) and $TaN/Ta_2O_5/Pt$ single layer (SL) devices on commercially thin (∼18μm) polyimide substrate. A 20 nm Ti adhesion layer was deposited and followed by a 100 nm Pt bottom electrode (BE) by E-beam evaporation. Hereafter, a 5 nm WO_3 layer and 20 nm Ta_2O_5 switching layer were deposited by RF and DC sputtering, respectively. The deposition parameters of both WO_3 and Ta_2O_5 were maintained with an Ar/O_2 gas mixture ratio of 3:1 and 2:1 with 50W and 300W power and working pressure of 10 and 5 mTorr, respectively. Finally, 50 nm TaN top electrode (TE) was patterned with a metal shadow mask (25 to 200 μm diameter) by DC sputtering. We used an Agilent B1500A semiconductor analyzer for the electrical measurement; voltage bias and

---

AQ:1 Manuscript received September 29, 2021; revised November 2, 2021; accepted November 4, 2021. This work was supported by the Ministry of Science and Technology, Taiwan, under Project MOST107-2221-E-009-089-MY3. The work of Debashis Panda was
AQ:2 supported by DST-SERB, GoI, under Grant SRG/2019/000129. The review of this letter was arranged by Editor S. Zhang. *(Corresponding author: Tseung-Yuen Tseng.)*

AQ:3 Sailesh Rajasekaran is with the Department of Materials Science and Engineering, National Yang Ming Chiao Tung University, Hsinchu 30010, Taiwan.

AQ:4 Firman Mangasa Simanjuntak and Tseung-Yuen Tseng are with the Institute of Electronics, National Yang Ming Chiao Tung University, Hsinchu 30010, Taiwan (e-mail: tseng@cc.nctu.edu.tw).

Sridhar Chandrasekaran is with the Advanced Research Institute, Dr. M. G. R. Educational and Research Institute, Chennai 600095, India.

Debashis Panda is with the Department of Physics, National Institute of Science and Technology, Berhampur 761008, India.

Aftab Saleem is with the Department of Electrical Engineering and Computer Science, National Yang Ming Chiao Tung University, Hsinchu 30010, Taiwan.

Color versions of one or more figures in this letter are available at https://doi.org/10.1109/LED.2021.3127489.

Digital Object Identifier 10.1109/LED.2021.3127489

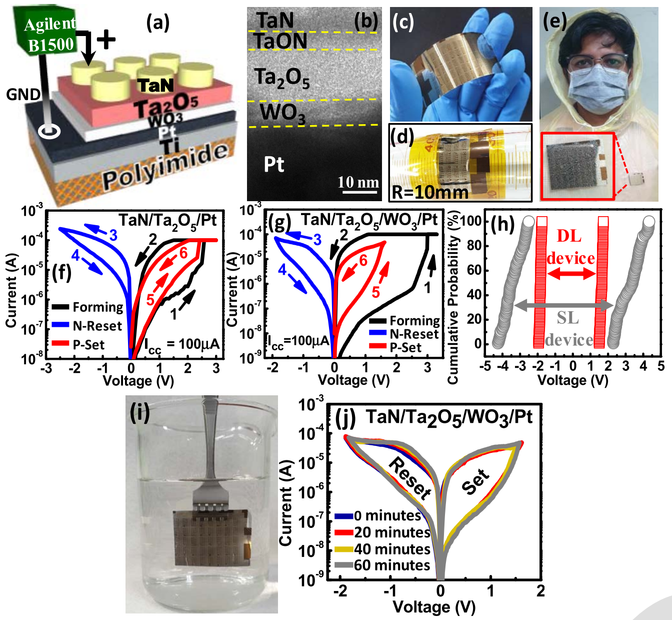

Fig. 1. (a) Schematic of TaN/Ta$_2$O$_5$/WO$_3$/Pt memristor synapse, (b) Cross-sectional TEM image of the DL device. Demonstration of DL device on (c) fingers, (d) R = 10mm test tube and (e) polymer coat. (f and g) Typical *I-V* curve of SL and DL devices along with forming process, (h) Operation voltage distributions of SL and DL devices, (i) devices being immersed in water, (j) I-V curve of the DL device after immersed in water (i).

amplitude were applied on TE while BE was grounded. The flexibility test was carried out using a mechanical bending machine (Sadhu design).

III. RESULTS AND DISCUSSION

The cross-sectional TEM image, shows in Fig. 1(b), indicating the TaON interfacial layer formation between the TaN and Ta$_2$O$_5$ layers. The flexibility of the fabricated devices were demonstrated on various arbitrary surfaces owing to the flexible substrate, as depicted in Figs. 1(c-e). The switching behavior of the devices are shown in Figs. 1(f and g). The forming voltage (V$_{\text{form}}$) of the DL device is slightly increased to 3V (V$_{\text{form}}$ of SL device is 2.33V) due to the insertion of WO$_3$ increases the oxide thickness. A 100 μA current compliance (I$_{\text{cc}}$) was used during the set process, and gradual switching is observed during both set/reset process in the DL device (full analog). Meanwhile, the SL device exhibits an abrupt set process indicating semi-analog behavior. The insertion of WO$_3$ decreases the set and reset voltages from 2.3 to 1.6V and -2.5 to -1.89V, respectively. Besides, the DL device exhibits narrower distribution for the consecutive switching cycles (Fig. 1(h)). Note that the DL device do not suffer from switching degradation even after immersed in water for about 1 hour (Fig. 1(i), thermally glued on polymer coat), confirming its water-resistant behavior (Fig. 1(j)).

The DL device performs superior non-volatility ($>10^6$ s) up to 200°C without any data loss, as shown in Fig. 2(a); DL device exhibits impressive pulse endurance (for more than 3×10^9 cycles with an ON/OFF ratio of about 1.5 orders) under flat and extreme bending conditions (R = 2 mm, 25 ns switching speed), as shown in Fig. 2(b). The inset of Fig. 2(b) shows the DL device fixed on a 2 mm circular object. We examined the flexibility of the SL and DL devices and the results are shown in Fig. 2(c). The DL device performs a stable operation up to 10^4 bending cycles (at R = 4 mm); meanwhile, the SL device degrades and can only sustain up to 2500 bending cycles. This is due to the formation of cracks on the SL device, as confirmed by the SEM images (inset of Fig. 2(c)). Moreover, the insertion of WO$_3$ layer improves mechanical adhesion on the Pt rather than Ta$_2$O$_5$ on the Pt, which conformed by peeling test using a scotch tape. We then explored the multilevel capability of the DL device, as shown in Fig. 2(d). The device can efficiently perform 3-bits states by varying the pulse width.

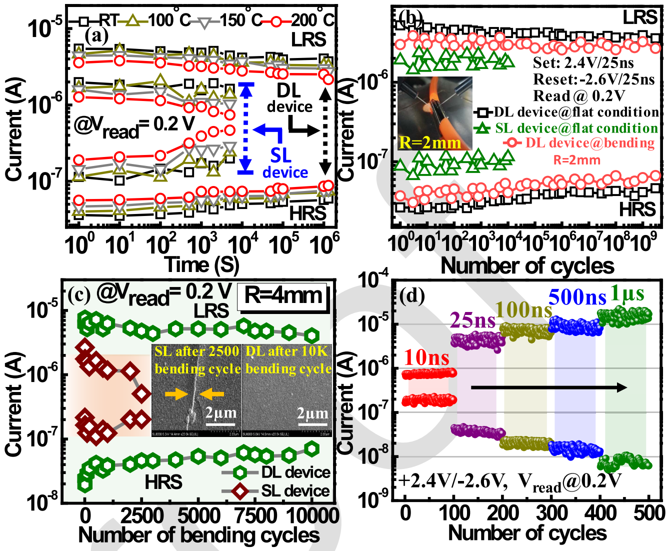

Fig. 2. (a) Data retention of SL and DL devices at different temperatures, (b) AC endurance test of SL and DL devices at flat and extreme bending radius = 2mm, and (c) DC endurance of the SL and DL devices after continous bending at R = 4mm. (d) Multilevel switching behavior of the DL device under various pulse width.

The synapse controls the transfer of information from presynaptic neurons to postsynaptic neurons in the mammalian brain, as illustrated in Fig. 3(a). SL device can only show synaptic behavior when a minimum amplitude of 2.2 V and -2.4 V were applied for potentiation (P) depression (D), respectively, as shown in Fig. 3(b). However, it exhibits an abrupt weight update during the first 18 μs and reaches saturation. In the case of DL device, the amplitude to trigger synaptic behavior is smaller (1.7 V and -1.9 V for P and D, respectively,) as shown in Fig. 3(c), and the DL device performs excellent gradual synaptic behavior. The DL device can perform stable epoch endurance (for more than 34 cycles) under extreme 2 mm bending. Note that the potentiation and depression in flat condition is as stable in bending condition. The synaptic nonlinearity of the DL and SL devices are measured according to the method reported by Wang *et al.* [23]. The synaptic nonlinearity of the DL device is improved to 0.64 (Fig. 3 (e)) from 0.80 of the SL device (not shown) at 2 mm bending. We further investigate the capability to control the linearity and dynamic range of the DL device employing various amplitudes and the results are shown in Figs. 3 (f) and (g); the DL device can exhibit an endless combination of low and high-weight updates during the synaptic operation at extreme 2 mm bending condition.

Based on the electron conduction analysis (curve fittings not shown) derived from the *I-V* curves (Figs. 1(f) and (g)),

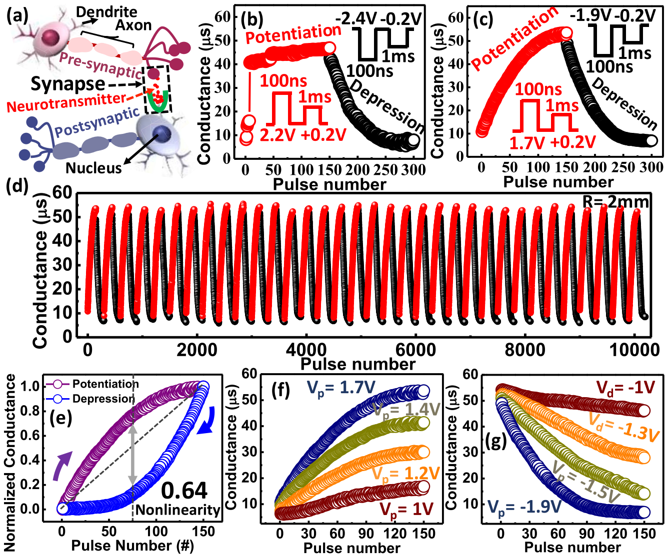

Fig. 3. (a) Schematic Illustration of an organic synapse. Synaptic measurement of potentiation/depression characteristics for (b) SL and DL devices (c). (d) stable 34 epochs trainings at 2 mm bending. (e) Nonlinearity curve with normalized conductance state for DL device at 2 mm bending. Different Pulse amplitude (f) potentiation and (g) depression at 2 mm bending employing 100 ns width and 1.1 ms interpulse.

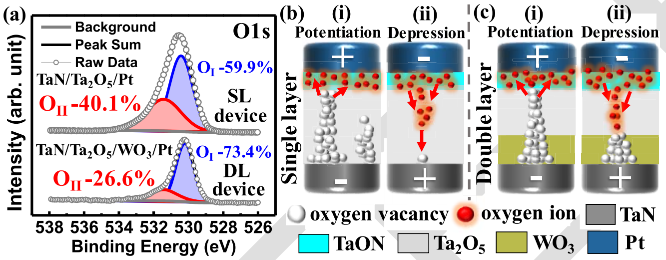

Fig. 4. (a) Depth-XPS spectra of O1s of Ta_2O_5 layer for DL device and SL devices). (b and c) Schematic of the conducting mechanism for SL and DL devices, respectively.

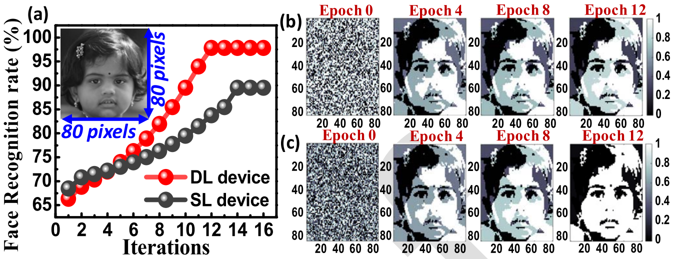

Fig. 5. (a) Neural network training accuracy of SL and DL devices (80 × 80 pixels input image in the insets). (b) and (c) evolution of image recognition during 0-12 epochs of SL and DL devices, respectively.

it indicates the typical filamentary conduction mechanism [24], which is the formation and rupture of the oxygen vacancy conductive filament (CF). We conducted XPS analysis to calculate the oxygen vacancy (Vo) concentration in the switching layer. Fig. 4(a) depicts the XPS spectra of O1s in Ta_2O_5 layers in DL and SL devices, respectively. The O_{II} peak corresponds to the non-lattice oxygen (Vo), which is higher (40.1%) in SL than that of the DL device (26.6%). This indicates that the Ta_2O_5 layer in SL has a higher oxygen vacancy. We infer that the Ta_2O_5 layer absorbs oxygen's from the WO_3 layer due to the lower Gibbs free energies of formation of Ta_2O_5 (-760 kj/mol) than that of WO_3 (-529 kj/mol), respectively [22]. Henceforth, the distribution of Vo difference in SL and DL devices may play a role in determining their behaviors.

We propose the conduction mechanism during synaptic operation of the SL and DL devices, as illustrated in Figs. 4(b) and (c), respectively. During potentiation of the SL, there is a high barrier at the Ta_2O_5/Pt (work function (Wf) of Ta_2O_5 and Pt are 4.05 and 5.65 eV, respectively) [25], [26] and require a high amplitude to initiate the potentiation; a high number of electrons flow into the Ta_2O_5 layer once the barrier is passed. Consequently, the accumulated electrons lead to the instant formation of Vo filament (Fig. 4(b)(i)) and, hence, the potentiation in SL occurs abruptly (Fig. 3(b)). During the depression, the TaON serves as oxygen reservoir which help to gradually ionized the oxygen's to recombine with filament [27].

The insertion of WO_3 layer in the DL device helps the initial formation of a filament in the switching layer (low pulse amplitude). The high intrinsic defects also help to reduce the barrier at the bottom interface (Wf of WO_3 is 4.8 eV [28]). Moreover, WO_3 has low thermal conductivity (1.63 W m^{-1} K^{-1}) that could minimize the contribution of Joule heating during the redox process, which assists a gradual ionization of oxygen's during potentiation (Fig.4(c)(i)). Note we infer that a small part of the filament that grow in the WO_x will remain after the depression and reset processes. This remnant acts as a seed to ease the redox process requiring smaller operating voltages and amplitudes and inducing stable switching and epoch endurance (Fig.4(c)(ii)) [18], [29].

We validated our synaptic devices for neuromorphic application by employing Hopfield neural network simulation to process 80 × 80 pixel binary image, as shown in Fig. 5. The Hopfield neural network is a recurrent neural network with neuron associated with each pixel in the binary image (0s and 1s). The neural network was trained with binary data of the image with a total of 6400 neurons associated for the simulation. Each neuron in the neural network undergoes summation and feedback logic on each iteration, once the neuron reaches desired states the logic is completed for the single pixel [18]. Thus, by repeating the computation sequence on each iteration can complete recognition of the binary image. The DL device is successfully recognizing the input image with 12 epoch trainings with 97.7% accuracy as depicted in Fig. 5 (a) while the SL device can only achieve 83.7% accuracy. The evolution of the face recognition at 0, 4th, 8th and 12th epoch for SL and DL device is depicted in Fig. 5 (b) and (c), respectively.

IV. CONCLUSION

This letter reports an extremely flexible Ta_2O_5/WO_3-based improved synaptic memristor with an excellent switching performance. The inserted WO_3 layer donates its oxygen to the Ta_2O_5 layer and makes the Ta_2O_5/WO_3 material system develops an oxygen-rich and oxygen-poor region that induces stable switching and synaptic operations with a lower operating voltages amplitude as compared to the SL control device. Consequently, the DL device performs higher endurance, lower operating voltages and faster learning even under extreme bending condition.

REFERENCES

[1] J. J. Harris, R. Jolivet, and D. Attwell, “Synaptic energy use and supply,” *Neuron*, vol. 75, no. 5, pp. 762–777, 2012, doi: 10.1016/j.neuron2012.08.019. AQ:5

[2] P. Yao, H. Wu, B. Gao, S. B. Eryilmaz, X. Huang, W. Zhang, Q. Zhang, N. Deng, L. Shi, H.-S. P. Wong, and H. Qian, “Face classification using electronic synapses,” *Nature Commun.*, vol. 8, no. 1, Aug. 2017, Art. no. 15199, doi: 10.1038/ncomms15199.

[3] J. Von Neumann, “The principles of large-scale computing machines,” *Ann. Hist. Comput.*, vol. 3, no. 3, pp. 263–273, Jul. 1981, doi: 10.1109/MAHC.1981.10025.

[4] M. Prezioso, F. Merrikh-Bayat, B. D. Hoskins, G. C. Adam, K. K. Likharev, and D. B. Strukov, “Training and operation of an integrated neuromorphic network based on metal-oxide memristors,” *Nature*, vol. 521, pp. 61–64, May 2015, doi: 10.1038/nature14441.

[5] Z. Wang, S. Joshi, S. E. Savel’ev, H. Jiang, R. Mindya, P. Lin, M. Hu, N. Ge, J. P. Strachan, Z. Li, Q. Wu, M. Barnell, G.-L. Xin, H. L. Xin, R. S. Williams, Q. Xia, and J. J. Yang, “Memristors with diffusive dynamics as synaptic emulators for neuromorphic computing,” *Nature Mater.*, vol. 16, no. 1, pp. 101–108, 2017, doi: 10.1038/nmat4756.

[6] Y. Shi, X. Liang, B. Yuan, V. Chen, H. Li, F. Hui, Z. Yu, F. Yuan, E. Pop, H.-S. P. Wong, and M. Lanza, “Electronic synapses made of layered two-dimensional materials,” *Nature Electron.*, vol. 1, no. 8, pp. 458–465, Aug. 2018, doi: 10.1038/s41928-018-0118-9.

[7] Q. Wu, H. Wang, Q. Luo, W. Banerjee, J. Cao, X. Zhang, F. Wu, Q. Liu, L. Li, and M. Liu, “Full imitation of synaptic metaplasticity based on memristor devices,” *Nanoscale*, vol. 10, no. 13, pp. 5875–5881, Feb. 2018, doi: 10.1039/c8nr00222c.

[8] F. M. Simanjuntak, T. Ohno, S. Chandrasekaran, T.-Y. Tseng, and S. Samukawa, “Neutral oxygen irradiation enhanced forming-less ZnO-based transparent analog memristor devices for neuromorphic computing applications,” *Nanotechnol.*, vol. 31, no. 26, Apr. 2020, Art. no. 26LT01, doi: 10.1088/1361-6528/ab7fcf.

[9] F. M. Simanjuntak, S. Chandrasekaran, C.-C. Lin, and T.-Y. Tseng, “ZnO_2/ZnO bilayer switching film for making fully transparent analog memristor devices,” *APL Mater.*, vol. 7, no. 5, May 2019, Art. no. 051108, doi: 10.1063/1.5092991.

[10] T. Wang, J. Meng, L. Chen, H. Zhu, Q. Sun, S. Ding, W. Bao, and D. W. Zhang, “Flexible 3D memristor array for binary storage and multi-states neuromorphic computing applications,” *InfoMat*, vol. 3, no. 2, pp. 212–221, Feb. 2021, doi: 10.1002/inf2.12158.

[11] T.-Y. Wang, J.-L. Meng, Q.-X. Li, Z.-Y. He, H. Zhu, L. Ji, Q.-Q. Sun, L. Chen, and D. W. Zhang, “Reconfigurable optoelectronic memristor for in-sensor computing applications,” *Nano Energy*, vol. 89, Nov. 2021, Art. no. 106291, doi: 10.1016/j.nanoen.2021.106291.

[12] Y. Park and J.-S. Lee, “Artificial synapses with short- and long-term memory for spiking neural networks based on renewable materials,” *ACS Nano*, vol. 11, no. 9, pp. 8962–8969, Sep. 2017, doi: 10.1021/acsnano.7b03347.

[13] J. Park, M. Kwak, K. Moon, J. Woo, D. Lee, and H. Hwang, “TiO_x-based RRAM synapse with 64-levels of conductance and symmetric conductance change by adopting a hybrid pulse scheme for neuromorphic computing,” *IEEE Electron Device Lett.*, vol. 37, no. 12, pp. 1559–1562, Aug. 2016, doi: 10.1109/LED.2016.2622716.

[14] S. Chandrasekaran, F. M. Simanjuntak, D. Panda, and T.-Y. Tseng, “Enhanced synaptic linearity in ZnO-based invisible memristive synapse by introducing double pulsing scheme,” *IEEE Trans. Electron Devices*, vol. 66, no. 11, pp. 4722–4726, Nov. 2019, doi: 10.1109/TED.2019.2941764.

[15] H. Tian, L. Zhao, X. Wang, Y.-W. Yeh, N. Yao, B. P. Rand, and T.-L. Ren, “Extremely low operating current resistive memory based on exfoliated 2D perovskite single crystals for neuromorphic computing,” *ACS Nano*, vol. 11, no. 12, pp. 12247–12256, Dec. 2017, doi: 10.1021/acsnano.7b05726. AQ:6

[16] B. Dang, Q. Wu, J. Sun, M. Zhao, S. Wang, F. Song, M. Yang, X. Ma, H. Wang, and Y. Hao, “Physically transient memristor synapse based on embedding magnesium nanolayer in oxide for security neuromorphic electronics,” *IEEE Electron Device Lett.*, vol. 40, no. 8, pp. 1265–1268, Aug. 2019, doi: 10.1109/LED.2019.2921322.

[17] M. Qi, S. Cao, L. Yang, Q. You, L. Shi, and Z. Wu, “Uniform multilevel switching of graphene oxide-based RRAM achieved by embedding with gold nanoparticles for image pattern recognition,” *Appl. Phys. Lett.*, vol. 116, no. 16, Apr. 2020, Art. no. 163503, doi: 10.1063/5.0003696.

[18] S. Chandrasekaran, F. M. Simanjuntak, R. Saminathan, D. Panda, and T.-Y. Tseng, “Improving linearity by introducing al in HfO_2 as a memristor synapse device,” *Nanotechnology*, vol. 30, no. 44, Nov. 2019, Art. no. 445205, doi: 10.1088/1361-6528/ab3480.

[19] A. Saleem, F. M. Simanjuntak, S. Chandrasekaran, S. Rajasekaran, T.-Y. Tseng, and T. Prodromakis, “Transformation of digital to analog switching in TaO_x-based memristor device for neuromorphic applications,” *Appl. Phys. Lett.*, vol. 118, no. 11, Mar. 2021, Art. no. 112103, doi: 10.1063/5.0041808.

[20] C.-H. Huang, J.-S. Huang, S.-M. Lin, W.-Y. Chang, J.-H. He, and Y.-L. Chueh, “ZnO_{1-x} nanorod arrays/ZnO thin film bilayer structure: From homojunction diode and high-performance memristor to complementary 1D1R application,” *ACS Nano*, vol. 6, no. 9, pp. 8407–8414, Sep. 2012, doi: 10.1021/nn303233r.

[21] S. Rajasekaran, F. M. Simanjuntak, D. Panda, S. Chandrasekaran, R. Aluguri, A. Saleem, and T.-Y. Tseng, “Fast, highly flexible, and transparent TaO_x-based environmentally robust memristors for wearable and aerospace applications,” *ACS Appl. Electron. Mater.*, vol. 2, no. 10, pp. 3131–3140, Oct. 2020, doi: 10.1021/acsaelm.0c00441.

[22] A. Prakash, S. Maikap, C. S. Lai, T. C. Tien, W. S. Chen, H. Y. Lee, F. T. Chen, M.-J. Kao, and M.-J. Tsai, “Bipolar resistive switching memory using bilayer TaO_x/WO_x films,” *Solid-State Electron.*, vol. 77, pp. 35–40, Nov. 2012, doi: 10.1016/j.sse.2012.05.028.

[23] I.-T. Wang, C.-C. Chang, L.-W. Chiu, T. Chou, and T.-H. Hou, “3D Ta/TaO_x/TiO_2/Ti synaptic array and linearity tuning of weight update for hardware neural network applications,” *Nanotechnology*, vol. 27, no. 36, Sep. 2016, Art. no. 365204, doi: 10.1088/0957-4484/27/36/365204.

[24] Y. C. Yang, F. Pan, Q. Liu, M. Liu, and F. Zeng, “Fully room-temperature-fabricated nonvolatile resistive memory for ultrafast and high-density memory application,” *Nano Lett.*, vol. 9, no. 4, pp. 1636–1643, Feb. 2009, doi: 10.1021/nl900006g.

[25] S. Ezhilvalavan and T. Tseng, “Electrical properties of Ta_2O_5 thin deposited on Cu,” *Thin Solid Films*, vol. 360, pp. 268–273, Feb. 2000, doi: 10.1016/S0040-6090(99)00873-1.

[26] H. B. Michaelson, “The work function of the elements and its periodicity,” *J. Appl. Phys.*, vol. 48, no. 11, pp. 4729–4733, 1977, doi: 10.1063/1.323539.

[27] L.-Y. Chang, F. M. Simanjuntak, C.-L. Hsu, S. Chandrasekaran, and T.-Y. Tseng, “Suboxide interface induced digital-to-analog switching transformation in all Ti-based memristor devices,” *Appl. Phys. Lett.*, vol. 117, no. 7, Aug. 2020, Art. no. 073504, doi: 10.1063/5.0014829.

[28] M. Y. Chan, C. S. Lee, S. L. Lai, M. K. Fung, F. L. Wong, H. Y. Sun, K. M. Lau, and S. T. Lee, “Efficient organic photovoltaic devices using a combination of exciton blocking layer and anodic buffer layer,” *J. Appl. Phys.*, vol. 100, no. 9, Nov. 2006, Art. no. 094506, doi: 10.1063/1.2363649.

[29] P.-Y. Jung, D. Panda, S. Chandrasekaran, S. Rajasekaran, and T.-Y. Tseng, “Enhanced switching properties in TaO_x memristors using diffusion limiting layer for synaptic learning,” *IEEE J. Electron Devices Soc.*, vol. 8, pp. 110–115, 2020, doi: 10.1109/JEDS.2020.2966799.